

Anisotropy of average potential energy of passive plate in bacterial suspensions

Luhui Ning(宁鲁慧), Ziwei Xiao(肖紫薇), Yuxin Tian(田宇鑫), Hongwei Zhu(朱红伟), Yi Peng(彭毅), Peng Liu(刘鹏), Ning Zheng(郑宁), Mingcheng Yang(杨明成), and Junqing Chen(陈君青)

Citation: Chin. Phys. B, 2025, 34 (**4**): 048201. DOI: 10.1088/1674-1056/adbee6
Journal homepage: http://cpb.iphy.ac.cn; http://iopscience.iop.org/cpb

What follows is a list of articles you may be interested in

Constraint dependence of average potential energy of a passive particle in an active bath

Simin Ye(叶思敏), Peng Liu(刘鹏), Zixuan Wei(魏子轩), Fangfu Ye(叶方富), Mingcheng Yang(杨明成), Ke Chen(陈科)
Chin. Phys. B, 2020, 29 (**5**): 058201. DOI: 10.1088/1674-1056/ab7d9b

Molecular dynamics simulations on the dynamics of two-dimensional rounded squares

Zhang-lin Hou(侯章林), Ying Ju(句颖), Yi-wu Zong(宗奕吾), Fang-fu Ye(叶方富), Kun Zhao(赵坤)
Chin. Phys. B, 2018, 27 (**8**): 088203. DOI: 10.1088/1674-1056/27/8/088203

Can secondary nucleation exist in ice banding of freezing colloidal suspensions?

Jia-Xue You(游家学), Jin-Cheng Wang(王锦程), Li-Lin Wang(王理林), Zhi-Jun Wang(王志军), Jun-Jie Li(李俊杰), Xin Lin(林鑫)
Chin. Phys. B, 2016, 25 (**12**): 128202. DOI: 10.1088/1674-1056/25/12/128202

Polydisperse spherical colloidal silica particles: Preparation and application

Hui Kong(孔慧), Junchao Huo(霍军朝), Chenliang Liang(梁晨亮), Shasha Li(李沙沙), Weili Liu(刘卫丽), Zhitang Song(宋志棠)
Chin. Phys. B, 2016, 25 (**11**): 118202. DOI: 10.1088/1674-1056/25/11/118202

Particles inside electrolytes with ion-specific interactions, their effective charge distributions and effective interactions

Mingnan Ding(丁茗楠), Yihao Liang(梁逸浩), Xiangjun Xing(邢向军)
Chin. Phys. B, 2016, 25 (**10**): 108201. DOI: 10.1088/1674-1056/25/10/108201

Anisotropy of average potential energy of passive plate in bacterial suspensions

Luhui Ning(宁鲁慧)[1,2,†], Ziwei Xiao(肖紫薇)[2], Yuxin Tian(田宇鑫)[3], Hongwei Zhu(朱红伟)[4], Yi Peng(彭毅)[5,6], Peng Liu(刘鹏)[3], Ning Zheng(郑宁)[3], Mingcheng Yang(杨明成)[5,6,7], and Junqing Chen(陈君青)[1,2,‡]

[1] *Beijing Key Laboratory of Optical Detection Technology for Oil and Gas, China University of Petroleum-Beijing, Beijing* 102249, *China*
[2] *Basic Research Center for Energy Interdisciplinary, College of Science, China University of Petroleum-Beijing, Beijing* 102249, *China*
[3] *School of Physics, Beijing Institute of Technology, Beijing* 100081, *China*
[4] *School of Physical Science and Technology, Key Laboratory of Magnetism and Magnetic Materials for Higher Education in Inner Mongolia Autonomous Region, Baotou Teachers' College, Baotou* 014030, *China*
[5] *Beijing National Laboratory for Condensed Matter Physics and Laboratory of Soft Matter Physics, Institute of Physics, Chinese Academy of Sciences, Beijing* 100190, *China*
[6] *University of Chinese Academy of Sciences, Beijing* 100049, *China*
[7] *Songshan Lake Materials Laboratory, Dongguan* 523808, *China*

(Received 20 January 2025; revised manuscript received 23 February 2025; accepted manuscript online 11 March 2025)

We conduct optical-tweezers experiments to investigate the average potential energies of passive plates harmonically trapped in bacterial suspensions. Our results show that the mean potential energies along both the major and minor axes increase with bacterial concentration but decrease with trap stiffness. Notably, the average potential energy along the major axis consistently exceeds that along the minor axis. This discrepancy from equilibrium systems is primarily attributed to the distinct bacterial flow fields and direct bacterium–plate collisions near the major and minor axes, as evidenced by the higher orientational order around the plate along the major compared to the minor axis, despite identical bacterial densities in these regions. Our findings highlight the critical role of hydrodynamic interactions in determining the potential energy of passive objects immersed in an active bath.

Keywords: average potential energy, active bath, passive plate, hydrodynamic interactions

PACS: 82.70.Dd, 87.16.Uv, 87.64.M–, 87.80.Cc

DOI: 10.1088/1674-1056/adbee6 **CSTR:** 32038.14.CPB.adbee6

1. Introduction

Active matter, consisting of self-propelling units that convert stored or environmental energy into mechanical motion, is ubiquitous in nature, biological and physical systems, including biological tissues,[1–3] bacterial colonies,[4–6] artificial nanomotors,[7–9] flocking birds,[10–12] and human crowds.[13–15] Unlike passive systems, active matter systems are inherently out of equilibrium at the level of individual constituents, giving rise to a range of novel behaviors absent in equilibrium systems, such as dynamic self-assembly,[16–18] motility-induced phase separation,[19–21] and collective motion.[22–25] Moreover, active matter significantly influences the behavior of immersed passive objects, leading to phenomena distinct from those of passive Brownian particles in thermal baths, including enhanced diffusion,[26–29] abnormal effective pressure and interactions,[30–33] and curvature-dependent accumulation.[34–36] Active systems, thus, provide experimental platforms for exploring and advancing theories of nonequilibrium physics due to their intrinsic nonequilibrium properties.

A fundamental result of equilibrium statistical mechanics is the energy equipartition theorem. In its basic form, each quadratic term in the Hamiltonian contributes an equal amount of energy, $0.5k_{\mathrm{B}}T$, to the system's average energy. For a colloidal harmonic oscillator in equilibrium, this applies equally to both kinetic and potential energies. Consequently, a Brownian colloidal particle can be used to probe the local potential by analyzing its position probability distribution, $U_x = U_y = \frac{1}{2}k_x\langle\Delta x^2\rangle = \frac{1}{2}k_y\langle\Delta y^2\rangle = 0.5k_{\mathrm{B}}T$, where Δx and Δy are the displacements from the particle's equilibrium position. Recently, there has been growing interest in the search for a generalized equipartition theorem in nonequilibrium systems, which has emerged as a hot topic.[37–39]

Maggi *et al*. demonstrated that the average potential energy of a passive spherical particle confined harmonically in a bacterial suspension depends on the stiffness of the trap,[38] which has been corroborated by both experiments and simulations.[39] The generalized equipartition theorem in active systems differs fundamentally from its equilibrium counterpart. Surprisingly, previous simulations that excluded hydrodynamic interactions can well reproduce experimental results for the average potential energy of spherical particles

†Corresponding author. E-mail: lhningphy@cup.edu.cn
‡Corresponding author. E-mail: cjq7745@163.com

© 2025 Chinese Physical Society and IOP Publishing Ltd. All rights, including for text and data mining, AI training, and similar technologies, are reserved.

in harmonic traps. This agreement suggests that bacterial collisions play a dominant role in determining the potential energy of spherical particles.[38,39] This conclusion appears counterintuitive, as the flows generated by active units significantly influence the effective interactions,[30] the self-organized structures and dynamics of both active and passive objects.[28,29,40,41] The seemingly inconsistent observations raise an intriguing question: how do hydrodynamic interactions fundamentally impact the average potential energy of particles in active fluids?

In this paper, we investigate the average potential energy of a plate harmonically trapped by optical tweezers in bacterial suspensions. Platelike objects are chosen for their ability to facilitate the alignment of active agents,[42–45] thereby enhancing hydrodynamic contributions. Our results reveal that the average potential energies along both the major and minor axes increase with bacterial concentration but decrease with trap stiffness, while the average potential energy along the major axis consistently exceeds that along the minor axis, which deviates from the prediction of the equilibrium equipartition theorem. Furthermore, video microscopy shows that bacterial alignment with the plate is higher along the major axis than that along the minor axis, while bacterial densities remain approximately equal between them. These findings suggest that the observed difference in average energy between the major and minor axes primarily arises from distinct bacterial flow fields and direct bacterium–plate collisions near the respective axes.

2. Experimental method

A dilute dispersion of plates, fabricated lithographically using SU-8 polymer[46] with dimensions of $(20.0 \times 7.5 \times 7.5)$ μm^3, is mixed into a suspension of *Escherichia coli* (*E. coli*) ($\sigma = 1.0 \pm 0.13$ μm in diameter, $l = 3.0 \pm 0.11$ μm in length, swimming at $v_{\mathrm{E}} = 10.8 \pm 0.88$ μm/s in deionized water).[30] A few polystyrene (PS) beads with a diameter of $\sigma = 10.0$ μm are added as spacers to ensure a uniform sample thickness of $\sigma = 10.0$ μm. The mixture is then sealed in a closed chamber to prevent chemotaxis and external fluid flows. Images are captured using a bright-field microscope (Nikon Ti-U) with a water-immersed 60× objective lens and a camera recording at 30 frames per second. The positions of both the plates and bacteria are extracted from the recorded images using customized particle tracking techniques.[47,48]

The plate is positioned in the focal plane of the microscope using optical tweezers (Aresis Tweez 250si) and is approximately centered in the z direction of the sample to prevent direct contact with either the top or bottom glass surfaces, as shown in Fig. 1(a). Figure 1(b) illustrates that eight optical tweezers (laser wavelength $\lambda = 1064$ nm) are used to hold the plate, preventing it from flipping during experiments. The plate is confined within an effective optical harmonic potential trap formed by the eight optical tweezers and exhibits slight fluctuations around the trap center. Displacements from the center of the trap in the x and y directions are denoted by Δx and Δy, respectively.

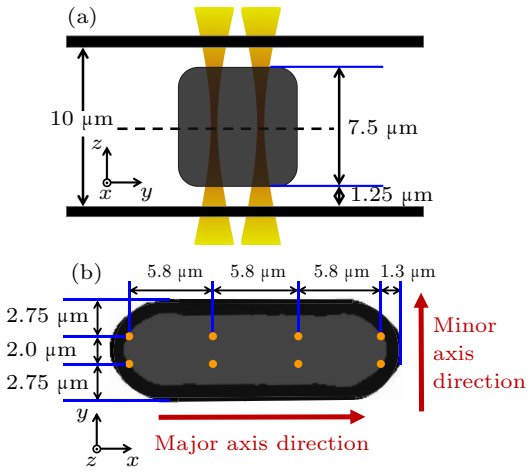


Fig. 1. (a) Schematic experimental setup with a plate (grey square) trapped between two cover slides (thick black lines) using eight optical tweezers. The observation plane, indicated by the black dashed line, is positioned at the optical waist of the tweezers. (b) Position distribution of the eight optical tweezers on the plate (grey ellipse-like with black edges) in the xy-plane, with orange circles marking the positions of the optical tweezers. The red arrows indicate the directions of the major and minor axes of the plate in the xy-plane.

The average potential energy of the plate in the x (along the major axis of the plate) and y (along the minor axis of the plate) directions is given by $U_x = \frac{1}{2}k_x\langle\Delta x^2\rangle$ and $U_y = \frac{1}{2}k_y\langle\Delta y^2\rangle$ in the linear region of the effective harmonic traps, respectively. Here, Δx^2 and Δy^2 represent the square distances between the plate's position and the center of the effective harmonic trap along the x and y axes, respectively, while k_x and k_y are the effective stiffness coefficients in these directions. The effective potential energies U_x and U_y are calculated from the plate positions recorded over 20000 frames. By varying the bacterial concentration and the laser intensity of the optical tweezers, we investigate the effects of bacterial packing fraction ϕ and stiffness coefficients k_x and k_y on the potential energies U_x and U_y.

3. Results and discussion

3.1. Effective stiffness coefficients k_x and k_y of the optical traps

The effective stiffness coefficients k_x and k_y of the optical traps, which depend on the laser intensity, can be calibrated by measuring the distribution of trapped plates in water without bacteria (in equilibrium). In thermal equilibrium, the potential energies, $U(\Delta x) = \frac{1}{2}k_x\Delta x^2$ and $U(\Delta y) = \frac{1}{2}k_y\Delta y^2$, of the plates follow the Boltzmann distribution, and Δx and Δy, representing the displacements of the plates from the trap center in the

x and y directions, follow the Gaussian distribution

$$P(\Delta x) \propto \exp\left(\frac{-U(\Delta x)}{k_{\mathrm{B}}T}\right) = \exp\left(\frac{-k_x \Delta x^2}{2k_{\mathrm{B}}T}\right), \quad (1)$$

$$P(\Delta y) \propto \exp\left(\frac{-U(\Delta y)}{k_{\mathrm{B}}T}\right) = \exp\left(\frac{-k_y \Delta y^2}{2k_{\mathrm{B}}T}\right). \quad (2)$$

Here, $k_{\mathrm{B}}T$ is the thermal energy. Figures 2(a) and 2(b) plot Δx and Δy distributions of the plate for different bacterial concentrations ϕ. In thermal equilibrium ($\phi = 0$), the distributions of Δx and Δy are accurately fitted to Eqs. (1) and (2), as shown by the solid black lines, from which the stiffness coefficients k_x and k_y can be extracted. However, due to the influence of the interactions from the bacterium–plate collisions and bacterial flow fields, the probability of the plate moving further from the trap center is higher than in the equilibrium case, and the range of motion increases with the bacterial concentration. This effect is less pronounced at low concentrations, where the distributions of Δx ($\phi = 0.043$) and Δy ($\phi = 0.043, 0.067$) still follow a Gaussian form, as shown by the red and blue lines in Figs. 2(a) and 2(b). As the bacterial concentration increases, the distributions of Δx ($\phi = 0.067, 0.093, 0.114$) and Δy ($\phi = 0.093, 0.114$) can no longer be well fitted by a Gaussian distribution, and the deviation from the Gaussian distribution becomes more noticeable with bacterial concentrations of $\phi = 0.093$, 0.114. Such non-Gaussian distributions are frequently observed in active systems.[38,39]

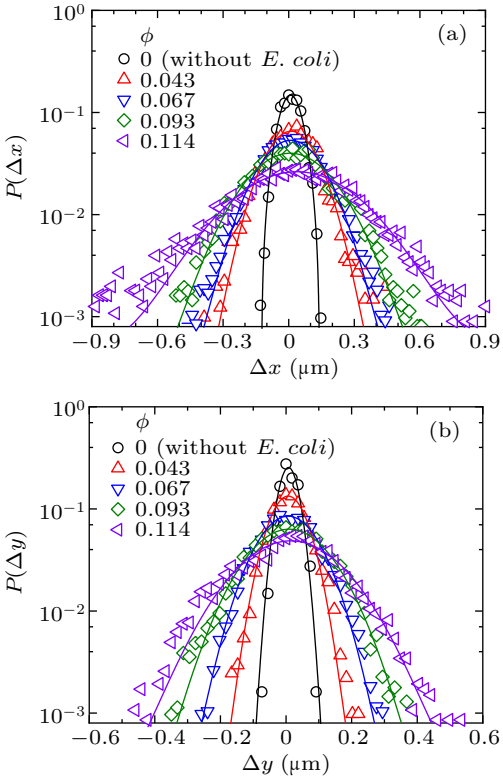


Fig. 2. The distributions of the displacement Δx and Δy of the plate from the trap center along the (a) x and (b) y directions at different bacterial concentrations ϕ. The symbols and solid lines represent the experimental data and the fitting curves of Eqs. (1) and (2), respectively.

The stiffness coefficients k_x and k_y are calibrated from four independent measurements by analyzing over 20000 frames of plate positions harmonically trapped in the absence of bacteria. Due to the unique structure of the plate and the different arrangements of the optical tweezers along the x and y directions (as shown in Fig. 1(b)), the same laser power results in different values for k_x and k_y in the two directions. By tuning the laser intensity, we obtained the following series of stiffness coefficients: $k_x = 1.38, 2.03, 3.17, 3.91, 5.12, 6.17, 7.18, 9.78$ pN/μm, and $k_y = 1.64, 2.52, 3.65, 5.45, 7.11, 7.66, 10.21, 12.63$ pN/μm.

3.2. Influence of stiffness coefficients k_x and k_y on the average potential energy U_x and U_y

Firstly, we investigated the effect of bacterial concentration on the normalized potential energy $U_x/k_{\mathrm{B}}T$ and $U_y/k_{\mathrm{B}}T$ of the plate with a constant laser intensity. k_x and k_y were calibrated to be k_x = 2.03 pN/μm and k_y = 3.65 pN/μm by analyzing the positions of the plate over 20000 frames without bacteria at a specific laser intensity. Figure 3(a) shows the normalized potential energy $U_x/k_{\mathrm{B}}T$ and $U_y/k_{\mathrm{B}}T$ of the plate as a function of the bacterial packing fraction $\phi = N \times S_{\mathrm{E}}/S_{\mathrm{tot}}$, where N is the bacterial number, $S_{\mathrm{E}} = (3.0 \times 1.0)$ μm^2 is the area of a single bacterium, and S_{tot} is the total area of the viewing field. In equilibrium (i.e., in the absence of bacteria), both U_x and U_y are equal to $0.5k_{\mathrm{B}}T$, indicating that the average potential energies of the plate are identical in both directions, consistent with the equipartition theorem of energy for equilibrium systems. As the bacterial concentration increases, the system moves away from equilibrium, leading to an increase in both $U_x/k_{\mathrm{B}}T$ and $U_y/k_{\mathrm{B}}T$, but with $U_x/k_{\mathrm{B}}T$ consistently exceeding $U_y/k_{\mathrm{B}}T$.

To understand the underlying causes of the differences in U_x and U_y of the plate, we conducted more detailed analysis of the influence of k_x and k_y on U_x and U_y, respectively. Figures 3(b) and 3(c) show the relations between the normalized average potential energy $U_x/k_{\mathrm{B}}T$ and $U_y/k_{\mathrm{B}}T$ of the plate and the optical trap stiffnesses k_x and k_y. In equilibrium, both U_x and U_y are equal to $0.5k_{\mathrm{B}}T$ and remain constant as k_x and k_y increase [Fig. 3(b)]. However, in the bacterial suspension, U_x and U_y decrease with the stiffnesses k_x and k_y, respectively [Fig. 3(c)], which is consistent with previous studies.[38,39] The effect of the active bath on the average potential energy U_x and U_y of a passive particle harmonically trapped can be theoretically analyzed by including an active colored noise term in the traditional overdamped Langevin equation[38,39,49]

$$\dot{\Delta x} = \mu_x F(\Delta x) + \eta_x^{\mathrm{T}} + \eta_x^{\mathrm{A}}. \quad (3)$$

Here, μ_x is the mobility of the passive plate, $F(\Delta x) = -k_x \Delta x$ is the restoring force exerted by the external trap, and Δx is the displacement of the passive particle from the trapped center. η_x^{T} refers to the thermal noise with $\left\langle \eta_{x\alpha}^{\mathrm{T}}(t)\eta_{x\beta}^{\mathrm{T}}(t')\right\rangle =$

$2D_x^{\mathrm{T}}\delta_{\alpha\beta}\delta(t-t')$, where $D_x^{\mathrm{T}}=\mu_x k_{\mathrm{B}}T$ is the diffusion coefficient of the passive plate due to the thermal bath. η_x^{A} represents the active noise and satisfies $\left\langle \eta_{x\alpha}^{\mathrm{A}}(t)\eta_{x\beta}^{\mathrm{A}}(t')\right\rangle = D_x^{\mathrm{A}}\delta_{\alpha\beta}\exp(-|t-t'|/\tau_x)/\tau_x$, where D_x^{A} denotes the active contribution to the particle diffusion coefficient characterizing the strength of active fluctuations, and τ_x is the correlation time of the active fluctuations. From Eq. (3), the displacements of the passive particle from the trapped center can be calculated as

$$\Delta x(t)=\Delta x(0)\,\mathrm{e}^{-\mu_x k_x t}+\mathrm{e}^{-\mu_x k_x t}\int_0^t(\eta_x^{\mathrm{T}}+\eta_x^{\mathrm{A}})\,\mathrm{e}^{-\mu_x k_x t'}\,\mathrm{d}t'. \quad (4)$$

The mean square of $\Delta x(t)$ is given by

$$\begin{aligned}\left\langle\Delta x^2(t)\right\rangle =\ & \frac{D_x^{\mathrm{T}}}{\mu_x k_x}(1-\mathrm{e}^{-2\mu_x k_x t})+\frac{D_x^{\mathrm{A}}}{\mu_x k_x}\frac{1}{1-(\mu_x k_x\tau_x)^2}\\ &\times\left[1-\mathrm{e}^{-2\mu_x k_x t}+\mu_x k_x\tau_x(2\,\mathrm{e}^{-t/\tau_x-\mu_x k_x t}\right.\\ &\left.-\mathrm{e}^{-2\mu_x k_x t}-1)\right], \end{aligned}\quad (5)$$

and the average potential energy of the passive plate along the x direction is

$$\begin{aligned}U_x(k_x) =\ & \frac{1}{2}k_x\lim_{t\to\infty}\left\langle\Delta x^2(t)\right\rangle=\frac{1}{2}k_{\mathrm{B}}T+\frac{D_x^{\mathrm{A}}}{2\mu_x}\frac{1}{1+\mu_x k_x\tau_x}\\ =\ & \frac{1}{2}k_{\mathrm{B}}T+\frac{A_x}{1+B_x k_x}. \end{aligned}\quad (6)$$

Following the same process, the average potential energy of passive plate along the y direction can be expressed by

$$U_y(k_y)=\frac{1}{2}k_{\mathrm{B}}T+\frac{D_y^{\mathrm{A}}}{2\mu_y}\frac{1}{1+\mu_y k_y\tau_y}=\frac{1}{2}k_{\mathrm{B}}T+\frac{A_y}{1+B_y k_y}. \quad (7)$$

Here, $k_{\mathrm{B}}T/2$ originates from thermal noise, $A_x=\frac{D_x^{\mathrm{A}}}{2\mu_x}$, $B_x=\mu_x\tau_x$, $A_y=\frac{D_y^{\mathrm{A}}}{2\mu_y}$, and $B_y=\mu_y\tau_y$ are the parameters of active noise. We used Eqs. (6) and (7) to fit the experimental data in Fig. 3(c), shown as the blue and red solid lines with $A_x=89894.99$ pN·μm, $B_x=277546.31$ μm/pN, $A_y=0.21$ pN·μm, and $B_y=0.84$ μm/pN. The noise parameters along the major axis (A_x,B_x) of the plate are much greater than those along the minor axis (A_y,B_y), indicating that the active fluctuation experienced by the plate along the major axis is much stronger than that along the minor axis, which leads to U_x being greater than U_y. In the absence of the bacteria, the active noise vanishes, and the parameters $A_x=B_x=A_y=B_y=0$. In this case, Eqs. (6) and (7) reduce to $U_x(k_x)=U_y(k_y)=k_{\mathrm{B}}T/2$, which corresponds to the equipartition theorem of energy widely used in equilibrium systems.

In the bacterial suspension, the dependence of the average potential energy of the passive plate on confinement can be explained by the interaction between the plate and surrounding bacteria. The passive plate, under the influence of thermal fluctuations, bacterium–plate collisions and bacterial flow fields, may deviate from the center of the optical trap. The maximum displacement of the passive plate from the trap center in the x direction, with the influence of bacterium–plate collisions and bacterial flow fields, is given by $\Delta x=F/k_x$. Due to the force balance between the applied force from bacterium–plate collisions and bacterial flow fields, F, and the restoring force $(F(\Delta x)=k_x\Delta x)$ from the optical trap, the active contribution to the average potential energy can be estimated as $\frac{1}{2}k_x\Delta x^2=F^2/(2k_x)$, which is negatively correlated with the effective stiffness coefficient k_x of the optical trap.

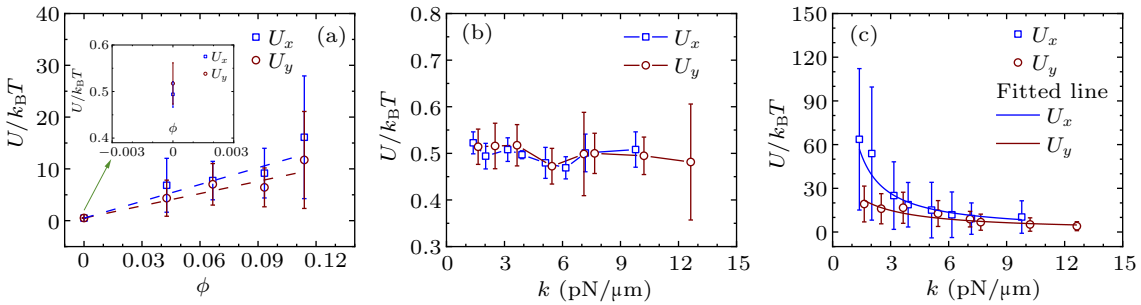


Fig. 3. Normalized average potential energy $U/k_{\mathrm{B}}T$ of plate along the x and y directions in optical traps. (a) The relation between $U_x/k_{\mathrm{B}}T$ and $U_y/k_{\mathrm{B}}T$ of the plate and bacterial concentration ϕ. The symbols and dashed lines represent the experimental data and linear fits, respectively. Inset: In equilibrium (without bacteria), both $U_x/k_{\mathrm{B}}T$ and $U_y/k_{\mathrm{B}}T$ are equal to 0.5. (b) In the absence of bacteria, $U_x/k_{\mathrm{B}}T$ and $U_y/k_{\mathrm{B}}T$ remain constant at 0.5 regardless of the optical coefficient k_x and k_y. (c) In the bacterial suspension with $\phi=0.14$, $U_x/k_{\mathrm{B}}T$ and $U_y/k_{\mathrm{B}}T$ decrease with increasing stiffness coefficients k_x and k_y. Hollow squares and circles represent the experimental data of $U_x/k_{\mathrm{B}}T$ and $U_y/k_{\mathrm{B}}T$, respectively, while the blue and red solid lines indicate the fitting curves of Eqs. (6) and (7) to the experimental data.

3.3. Impact of bacterial flow fields and bacterial collisions on the average potential energy U_x and U_y

However, unlike the equilibrium state, the average potential energy of the plate in the x direction (along the major axis) consistently exceeds that in the y direction (along the minor axis) at different constraints k_x and k_y, which is consistent with the results for U_x and U_y obtained at various bacterial concentrations [Fig. 3(a)]. To better understand the microscopic origins of this anisotropy in the average potential energy, we investigate the spatial density distributions and orientation order of bacteria surrounding the plate along the major and minor axes. The local density and orientation order are measured within a series of rectangular bins (7.5×4.6) μm^2 parallel to the major and minor axes of the plate at different X and Y posi-

tions, as shown in Fig. 4(c). The blue and yellow dashed boxes correspond to the rectangular bins parallel to the major axis (Y change) and minor axis (X change) of the plate, respectively. The relative density, $\rho_{\rm r} = \rho_{\rm loc}/\overline{\rho} = n \cdot S_{\rm bin}/(N_{\rm tot} \cdot S_{\rm totbin})$, is the ratio of the local density ($\rho_{\rm loc}$) to the average density ($\overline{\rho}$). Here, n represents the local bacterial count in a rectangular bin, $S_{\rm bin} = (7.5 \times 4.6)$ μm^2 is the bin area, $N_{\rm tot} = \sum n$ is the total bacterial count, and $S_{\rm totbin} = \sum S_{\rm bin}$. The local orientational order is defined as $Q = \langle|\cos\theta_x|\rangle$ (along the major axis) and $Q = \langle|\cos\theta_y|\rangle$ (along the minor axis),[30] where θ_x (θ_y) represents the angle of the bacterial body relative to the plate along the major (minor) axis, and $\langle\ \rangle$ denotes the ensemble average.

Figures 4(a) and 4(b) show $\rho_{\rm r}$ and Q as functions of position for different k_x and k_y. For all k_x and k_y, the bacterial number density and orientational order near the plate surfaces are significantly higher than in other regions, indicating that bacteria tend to accumulate near the plates and swim parallel to them.[30,42] However, the orientation of bacteria along the major axis of the plate (Y change) is consistently higher than that along the minor axis (X change), regardless of whether k_x is close to k_y [Fig. 4(a)] or there is a significant difference between them [Fig. 4(b)], indicating that bacteria exhibit a stronger preference for swimming parallel to the major axis of the plate.

In the bacterial suspension, the plate deviates from its equilibrium position due to the combined effects of thermodynamic energy $k_{\rm B}T$, bacterium–plate collisions, and bacterial flow fields. There is no significant difference in thermodynamic energy $k_{\rm B}T$ [Fig. 3(b)] and bacterial concentration $\rho_{\rm r}$ [Figs. 4(a) and 4(b)] along the major and minor axes of the plate. However, a notable difference in the local bacterial orientational order Q is observed between the axes [Figs. 4(a) and 4(b)]. Thus, the difference in plate positions fluctuations along the major and minor axes is primarily driven by the bacterial flow field and bacterium–plate collisions. First, as bacteria tend to move preferentially along the major axis of the plate, a flow field is generated near faces (3) and (4) of the plate [Fig. 4(c)], resulting in a drag force along the major axis. Second, the probability of bacterial collisions with faces (1) and (2) is slightly higher than with faces (3) and (4), due to a lower local orientational order Q along the minor axis but the identical bacterial relative density $\rho_{\rm r}$ along both axes. These factors result in more pronounced perturbations along the major axis of the plate, causing greater displacement of the plate along the major axis, i.e., Δx is greater than Δy. Consequently, the average potential energy along the major axis $U_x = \frac{1}{2}k_x\langle\Delta x^2\rangle$ is larger than the potential energy along the minor axis $U_y = \frac{1}{2}k_y\langle\Delta y^2\rangle$.

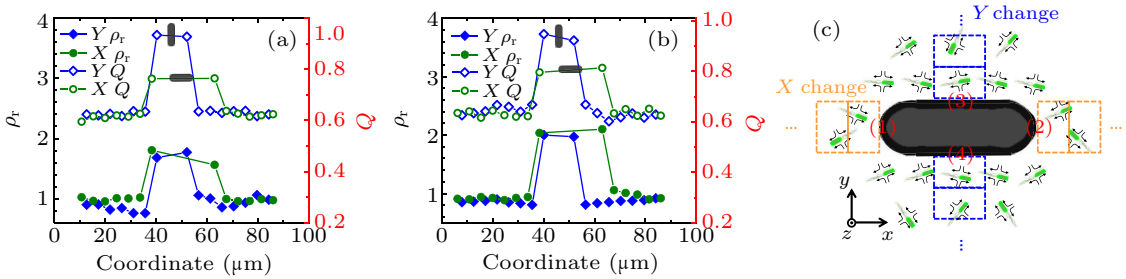


Fig. 4. Distributions of bacterial relative density $\rho_{\rm r}$ and local orientational order Q along the major and minor axes of the plate at different X and Y positions for the stiffnesses of (a) $k_x = 7.18$ pN/μm, $k_y = 7.11$ pN/μm, and (b) $k_x = 2.03$ pN/μm, $k_y = 3.65$ pN/μm. Solid and hollow symbols represent $\rho_{\rm r}$ and Q, respectively. The positions of the plate are indicated by the grey-shaded regions with black edges. (c) Sketch of the difference in bacterial flow field along the major and minor axes of the plate. The blue and yellow dashed boxes represent the rectangular bins (7.5×4.6) μm^2 parallel to the major axis (Y change) and minor axis (X change) of the plate, respectively.

4. Conclusion

In summary, we investigate the average potential energy of a passive plate trapped in harmonic wells within active *E. coli* suspensions. The average potential energies, U_x and U_y, increase with the bacterial packing fraction ϕ and decrease with the restraint intensities k_x and k_y, respectively. Bacteria exhibit a preference for swimming along the major axis of the plate compared to the minor axis, despite having identical bacterial relative density along both axes. Incorporating the characteristics of bacterial flow fields, the drag force on the plate along the major axis is greater than along the minor axis. Additionally, the probability of bacterial collisions with the minor axis of the plate is slightly higher than that with the major axis. As a result, the plate experiences a greater range of motion along the major axis. Consequently, the effective potential energy of the plate along the major axis (x direction) is consistently higher than that along the minor axis (y direction). This property, which significantly deviates from the equipartition theorem in equilibrium systems, is driven by the impact of bacterial flow fields and bacterial collisions in active nonequilibrium systems. Our findings emphasize the significant role of hydrodynamics in shaping the potential energy of passive particles in active nonequilibrium systems.

Acknowledgements

We acknowledge the supports of the National Natural Science Foundation of China (Grant Nos. 12304245, 12374205, 12475031, and 12364029), the Science Foun-

dation of China University of Petroleum, Beijing (Grant Nos. 2462023YJRC031 and 2462024BJRC010), the National Key Laboratory of Petroleum Resources and Engineering (Grant No. PRE/DX-2407), the Natural Science Foundation of Shandong Province (Grant No. ZR2024YQ017), the Young Elite Scientist Sponsorship Program by BAST (Grant No. BYESS2023300), and the Beijing Institute of Technology Research Fund Program for Young Scholars. This work was also supported by Beijing National Laboratory for Condensed Matter Physics (Grant Nos. 2023BNLCMPKF014 and 2024BNLCMPKF009).

References

[1] Riedel I H, Kruse K and Howard J 2005 *Science* **309** 300
[2] Friedrich B M and Jülicher F 2007 *Proc. Natl. Acad. Sci. USA* **104** 13256
[3] Rigato A, Miyagi A, Scheuring S and Rico F 2017 *Nat. Phys.* **13** 771
[4] Tailleur J and Cates M E 2008 *Phys. Rev. Lett.* **100** 218103
[5] Peruani F, Starruß J, Jakovljevic V, Søgaard-Andersen L, Deutsch A and Bär M 2012 *Phys. Rev. Lett.* **108** 098102
[6] Wioland H, Woodhouse F G, Dunkel J, Kessler J O and Goldstein R E 2013 *Phys. Rev. Lett.* **110** 268102
[7] Huang Y, Lin Z and He Q 2024 *Adv. Funct. Mater.* **34** 2311136
[8] Liu J, Wu Y, Li Y, Yang L, Wu H and He Q 2023 *Sci. Adv.* **9** eabg3015
[9] Palacci J, Sacanna S, Steinberg A P, Pine D J and Chaikin P M 2013 *Science* **339** 936
[10] Cavagna A, Cimarelli A, Giardina I, Parisi G, Santagati R, Stefanini F and Viale M 2010 *Proc. Natl. Acad. Sci. USA* **107** 11865
[11] Bialek W, Cavagna A, Giardina I, Mora T, Silvestri E, Viale M and Walczak A M 2012 *Proc. Natl. Acad. Sci. USA* **109** 4786
[12] Pearce D J, Miller A M, Rowlands G and Turner M S 2014 *Proc. Natl. Acad. Sci. USA* **111** 10422
[13] Rio K W, Dachner G C and Warren W H 2018 *Proc. Natl. Acad. Sci. USA* **285** 20180611
[14] Bottinelli A, Sumpter D T J and Silverberg J L 2016 *Phys. Rev. Lett.* **117** 228301
[15] Low D J 2000 *Nature* **407** 465
[16] Tan H, Yu C, Lu Z, Zhou Y and Yan D 2017 *Soft Matter* **13** 6178
[17] Soto R and Golestanian R 2014 *Phys. Rev. Lett.* **112** 068301
[18] Shi X Q, Fausti G, Chaté H, Nardini C and Solon A 2020 *Phys. Rev. Lett.* **125** 168001
[19] Digregorio P, Levis D, Suma A, Cugliandolo L F, Gonnella G and Pagonabarraga I 2018 *Phys. Rev. Lett.* **121** 098003
[20] Caprini L, Marini Bettolo Marconi U and Puglisi A 2020 *Phys. Rev. Lett.* **124** 078001
[21] Omar A K, Klymko K, GrandPre T and Geissler P L 2021 *Phys. Rev. Lett.* **126** 188002
[22] Sokolov A and Aranson I S 2012 *Phys. Rev. Lett.* **109** 248109
[23] Liu P, Zhu H, Zeng Y, Du G, Ning L, Wang D, Chen K, Lu Y, Zheng N, Ye F, *et al.* 2020 *Proc. Natl. Acad. Sci. USA* **117** 11901
[24] Großmann R, Aranson I S and Peruani F 2020 *Nat. Commun.* **11** 1
[25] Keta Y E, Fodor E, van Wijland F, Cates M E and Jack R L 2021 *Phys. Rev. E* **103** 022603
[26] Leptos K C, Guasto J S, Gollub J P, Pesci A I and Goldstein R E 2009 *Phys. Rev. Lett.* **103** 198103
[27] Guzmán-Lastra F, Löwen H and Mathijssen A J 2021 *Nat. Commun.* **12** 1
[28] Wu X L and Libchaber A 2000 *Phys. Rev. Lett.* **84** 3017
[29] Peng Y, Lai L, Tai Y S, Zhang K, Xu X and Cheng X 2016 *Phys. Rev. Lett.* **116** 068303
[30] Ning L, Lou X, Ma Q, Yang Y, Luo N, Chen K, Meng F, Zhou X, Yang M and Peng Y 2023 *Phys. Rev. Lett.* **131** 158301
[31] Liu P, Ye S, Ye F, Chen K and Yang M 2020 *Phys. Rev. Lett.* **124** 158001
[32] Feng F, Lei T and Zhao N 2021 *Phys. Rev. E* **103** 022604
[33] Liu P, Li L, Ning L, Zheng N and Yang M 2023 *J. Phys.: Condens. Matter* **35** 445102
[34] Mallory S A, Valeriani C and Cacciuto A 2014 *Phys. Rev. E* **90** 032309
[35] Kaiser A, Wensink H H and Löwen H 2012 *Phys. Rev. Lett.* **108** 268307
[36] Hua Y, Li K, Zhou X, He L and Zhang L 2018 *Soft Matter* **14** 5205
[37] To K 2014 *Phys. Rev. E* **89** 062111
[38] Maggi C, Paoluzzi M, Pellicciotta N, Lepore A, Angelani L and Di Leonardo R 2014 *Phys. Rev. Lett.* **113** 238303
[39] Ye S, Liu P, Wei Z, Ye F, Yang M and Chen K 2020 *Chin. Phys. B* **29** 058201
[40] Bechinger C, Di Leonardo R, Löwen H, Reichhardt C, Volpe G and Volpe G 2016 *Rev. Mod. Phys.* **88** 045006
[41] Zhang B, Leishangthem P, Ding Y and Xu X 2021 *Proc. Natl. Acad. Sci. USA* **118** e2100145118
[42] Drescher K, Dunkel J, Cisneros L H, Ganguly S and Goldstein R E 2011 *Proc. Natl. Acad. Sci. USA* **108** 10940
[43] Berke A P, Turner L, Berg H C and Lauga E 2008 *Phys. Rev. Lett.* **101** 038102
[44] Molaei M, Barry M, Stocker R and Sheng J 2014 *Phys. Rev. Lett.* **113** 068103
[45] Bianchi S, Saglimbeni F and Di Leonardo R 2017 *Phys. Rev. X* **7** 011010
[46] Hernandez C J and Mason T G 2007 *J. Phys. Chem. C* **111** 4477
[47] Crocker J C and Grier D G 1996 *J. Colloid Interface Sci.* **179** 298
[48] Zheng Z and Han Y 2010 *J. Chem. Phys.* **133** 124509
[49] Ye S, Liu P, Ye F, Chen K and Yang M 2020 *Soft Matter* **16** 4655